HAL open science

Probing biolubrication with a nanoscale flow

Sylvie Leroy, A. Steinberger, Cécile Cottin-Bizonne, Ana-Maria Sfarghiu, Elisabeth Charlaix

To cite this version:

Sylvie Leroy, A. Steinberger, Cécile Cottin-Bizonne, Ana-Maria Sfarghiu, Elisabeth Charlaix. Probing biolubrication with a nanoscale flow. Soft Matter, 2009, 5 (24), pp.4997-5002. 10.1039/B914543E . hal-00466921

HAL Id: hal-00466921

https://hal.science/hal-00466921v1

Submitted on 18 Nov 2022

HAL is a multi-disciplinary open access archive for the deposit and dissemination of scientific research documents, whether they are published or not. The documents may come from teaching and research institutions in France or abroad, or from public or private research centers.

L'archive ouverte pluridisciplinaire **HAL**, est destinée au dépôt et à la diffusion de documents scientifiques de niveau recherche, publiés ou non, émanant des établissements d'enseignement et de recherche français ou étrangers, des laboratoires publics ou privés.

Distributed under a Creative Commons Attribution - NonCommercial 4.0 International License

Probing biolubrication with a nanoscale flow

S. Leroy,*[ab] A. Steinberger,[ab] C. Cottin-Bizonne,[ab] A.-M. Trunfio-Sfarghiu[ab] and E. Charlaix*[ab]

The fluidity of lipid membranes is an essential property for their biological function. Here we use a dynamic surface forces apparatus to probe flow at the nanoscale on supported phospholipid bilayers and we present direct mechanical measurements of their fluidity. We show that gel-phase DPPC bilayers deposited on glass behave as a rigid surface for the flow, whereas fluid DOPC bilayers are mobile and slide with a very low friction coefficient. These findings provide new perspectives for the investigation of the lubricant properties of phospholipid bilayers and for the design of biomaterial and biomedical devices of low frictional properties.

I. Introduction

Substrate-supported lipid bilayers (SLBs) provide unique possibilities for reconstituting biological cell membranes on solid surfaces and have therefore an immense interest for nanobiotechnology applications.[1] They offer the appropriate host environment to study membrane proteins at the level of the single molecule and provide ideal analytical platforms for drug development.[2,3] They are ubiquitous in biological rubbing contacts and their unique lubricant properties hold great promise for biomedical materials, new artificial organs and implants.[4–6]

In all these applications the mechanical behaviour of SLBs is a key issue, as the bilayer fluidity is essential for mimicking the cell surface, maintaining its biological function and avoiding the denaturation of embedded proteins.[1] Like all soft and ultra-thin films resting on a solid interface, the mechanical properties of SLBs are difficult to probe directly. The existing methods for probing the fluidity of supported membranes rely essentially on lipid diffusion measurements using fluorescence-recovery-after-photobleaching (FRAP)[7–9] or NMR,[10] the diffusion coefficient being related through hydrodynamic calculations to the internal viscosity of the bilayer and its friction coefficient on the substrate.[11] The interpretation of such experiments is however non-trivial and rather involved, and the results are strongly affected by external parameters such as the area per lipid head.[12,13] Recently Jonsson *et al.* presented a first direct measurement of the mechanical response of a SLB to a shear stress, using an original microfluidic technique.[14]

We present here another direct determination of the fluidity of SLBs, thanks to a unique nanorheology technique using a dynamic surface forces apparatus (DSFA). By measuring the nanometric slippage of a SLB supported on a Pyrex substrate under a tangential shear stress, we determine its friction coefficient on the solid surface. These measurements provide a mechanical signature of the rigidity of gel phase DPPC (L-α-dipalmitoylphosphatidylcholine) supported bilayers and of the fluidity of DOPC (L-α-dioleoylphosphatidylcholine) ones. We find that the latter slides with a very low friction coefficient. Furthermore we correlate the tangential rigidity of the SLB and its ability to sustain a normal stress without rupture, a feature of high relevance for the lubricating properties of SLBs.[15,16]

II. Experimental

Our nanorheology technique is a surface force apparatus specifically designed for investigating the dynamics of liquids at interfaces.[17] Water is confined between a plane supporting the bilayer and a Pyrex sphere (see Fig. 1). The device oscillates the sphere at a very small amplitude so that its displacement normal to the plane is $D(t) = D + h_o\cos\omega t$ (0.1 nm < h_0 < 2 nm), and it measures the components of the responding force, *i.e.* the quasi-static component $F_{stat}(D)$ and the complex component $\tilde{F}(\omega)$ at the driving frequency $\omega/2\pi$. The quantity of interest for probing the response of the bilayer is the sphere mobility $\mu(D)$, defined as the ratio of the sphere velocity to the viscous drag induced by the flow. If the surfaces limiting the flow are rigid and enforce a no-slip boundary condition, the viscous force is the so-called Reynolds force and the mobility is proportional to the sphere-plane distance:

$$\mu(D) = -\frac{h_o\omega}{Im[\tilde{F}(\omega)]} = \frac{D}{6\pi\eta_w R^2} \quad (1)$$

with η_w the viscosity of water and R the sphere radius. Any deviation from this linear dependence reflects a finite motion of

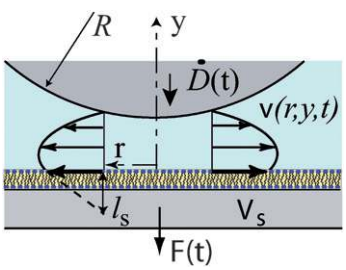

Fig. 1 Representation of a Poiseuille flow between a sphere and a fluid bilayer. The sliding velocity of the top of the bilayer is V_s. The apparent Navier slip length l_s is the ratio of the boundary velocity to the local shear $l_s = V_s/(\partial v/\partial z)_{bilayer}$.

[a] *Université de Lyon, F-69000, France*
[b] *Univ. Lyon 1 Laboratoire PMCN, CNRS, UMR 5586, F-69622 Villeurbanne Cedex, France. E-mail: Samuel.Leroy@lpmcn.univ-lyon1.fr; elisabeth.charlaix@lpmcn.univ-lyon1.fr*

the flow boundary, and possibly a deformation of the bilayer under the applied shear stress (see Appendix).

We study solid and fluid SLBs prepared using respectively DPPC and DOPC (Avanti Polar Lipids). These phospholipid bilayers have been shown to be respectively in a solid or gel phase (DPPC) and in a fluid phase (DOPC) at ambient temperature. More specifically, the lipid diffusion coefficient at room temperature measured by FRAP[7,18] is known to be much smaller in DPPC supported bilayers ($\simeq 10^{-12}$ cm^2/s) than in DOPC ones ($\simeq 10^{-8}$ cm^2/s), and the lipid packing density at room temperature measured by ellipsometry, X-ray scattering or neutron reflectivity is larger in DPPC bilayers (*i.e.*, about 50 Å^2 area per molecule) than in DOPC bilayers (*i.e.*, about 87 Å^2 area per molecule).[19,20]

The bilayers are deposited on clean hydrophilic floated Pyrex surfaces, stored in ultra-pure water (Millipore, milliQ, 18.2 MΩ.cm), and used within the day. DPPC bilayers are prepared at high lateral pressure (40 mN/m) by the Langmuir-Blodgett method using a standard procedure.[21] DOPC bilayers are formed with the method of co-adsorption of lipid-surfactant micelles.[19,22] We choose this method because it minimizes the risk of oxidation of the DOPC hydrophobic chains by exposure to air, as oxidation is known to have a strong impact on the fluid character of the bilayers. Lipids are solubilized together with 1% fluorescent lipids (DHPE-TRITC lipids from Molecular Probes, whose ends are fluorescent in green light) in chloroform/ethanol solvent in volume proportion 9/1. Solvent is evaporated with nitrogen on the wall of a tube, and the lipids are then allowed to hydrate in ultra-pure water to form a multi-lamellar vesicle suspension (2 g/L). The lipids are solubilized with the surfactant n-dodecyl-β-D-maltoside (DDM) in micelles (ratio 1/6 by weight) in water. 3 ml of micelle solution are co-adsorbed on a borosilicate glass plane for 5 min with 0.3 ml of a 20 mM $CaCl_2$ solution. Finally a long and slow rinsing with ultra-pure water is performed in order to remove the DMM, as explained in ref. 19. The lipid packing density, according to the determination of Grant *et al.* by ellipsometry, is about 90 Å^2 area per molecule.

We check the quality of our SLBs with an atomic force microscope (Veeco Explorer) used in the contact mode (Fig. 2). They appear smooth (less than 0.2 nm r.m.s. roughness on a 1μm × 1μm scan) and do not reveal defects. We showed in other works[16] in agreement with the literature[19] that the thickness of the bilayers e is 3.5–4 nm for the DOPC SLB and about 5 nm for the DPPC SLB. This difference can be explained by the different phases of these bilayers.

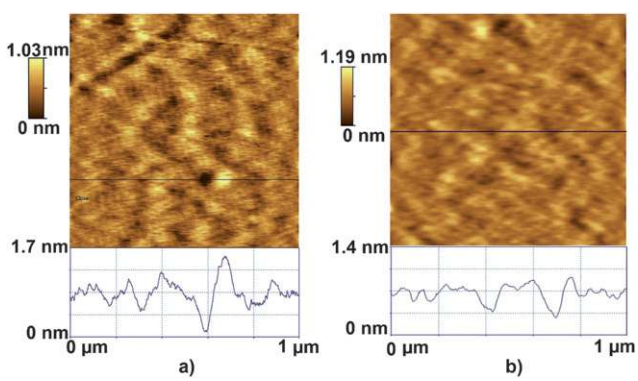

Fig. 2 AFM image and topography profile in contact mode of (**a**) a DOPC and (**b**) a DPPC bilayer immersed in water.

III. Results

Fig. 3 shows the results of nanorheology experiments on a DPPC bilayer. The static interaction force F_{stat} shows a steric repulsion when the Pyrex sphere comes into proximity with the bilayer, followed by a steep hard wall. On the backward motion a weak adhesion is observed. There is no sign of any bilayer degradation even at much higher load than the one applied in Fig. 3. The sphere mobility $\mu(D)$ varies as a straight line as a function of the sphere-plane distance in good agreement with eq (1), showing that a no-slip condition holds both on the sphere and on the bilayer. These data show the absence of water slippage at the DPPC/water interface as well as the absence of any significant tangential motion of the top of the DPPC bilayer with respect to its supporting substrate. The DPPC bilayer behaves as a rigid surface, and this up to the maximum tangential stress

$$\sigma_T = \eta_w \frac{\partial v_T}{\partial z}\bigg|_{max} \simeq 100 \text{ Pa}$$

probed in the experiment (see Appendix).

The intersection of the plot of $\mu(D)$ with the D-axis corresponds to the hydrodynamic origin, *i.e.* the contact between the flow boundaries, here the sphere/water and the DPPC/water interfaces. Choosing this hydrodynamic contact as the distance origin, the location of the steep hard wall occurs at an abscissa 0 ± 0.5 nm, while the onset of the steric repulsion occurs at a distance $D_s = 1 \pm 0.5$ nm when the sphere and the bilayer are still separated by a thin water film (Fig. 4). This thickness D_s is slightly larger than the peak-to-peak value of the roughness of the bilayer over a 1 μm^2 area. From the inset of Fig. 3 one sees that water remains fluid in this thin film without any noticeable change from its bulk viscosity.

The DOPC supported bilayers have a very different behaviour. On the first approach of the sphere, the mobility varies linearly with the displacement only at distances larger than about 15 nm from the bilayer. At smaller distances the plot deviates from the straight line and curves down to point towards a hydrodynamic

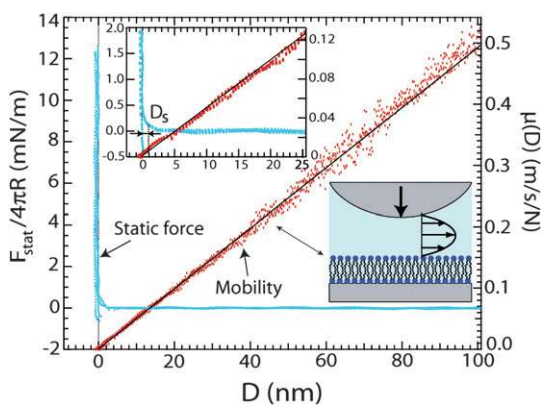

Fig. 3 Static force F_{stat} and sphere mobility as a function of the sphere-plane distance, obtained on a DPPC bilayer. The sphere radius is $R = 2.9 \pm 0.3$ mm and the frequency 19 Hz. The straight line is the best fit of the damping.

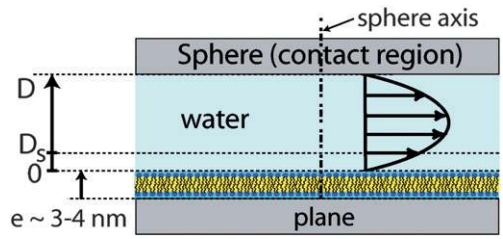

Fig. 4 Schematic representation of the flow of water on a DPPC bilayer and the associated distances. The origin of distances corresponds to the hydrodynamic contact between the sphere and the bilayer. The onset of the steric repulsion occurs at the distance $D_s = 1 \pm 0.5$ nm from hydrodynamic contact, through a fluid water film of similar viscosity as bulk water.

origin (Fig. 5). This origin locates the contact between the flow boundaries *i.e.* the sphere/water and DOPC/water interfaces, and is choosen as the distance origin. One sees on the static force that the steep hard wall repulsion is located beyond the hydrodynamic origin at a distance $e = 3 \pm 0.5$ nm equivalent to the bilayer thickness. Thus there is no steep repulsion between the sphere and the bilayer, the latter deforms and ruptures under the load applied by the sphere, leading to a strong adhesion when the sphere is separated from the plane.

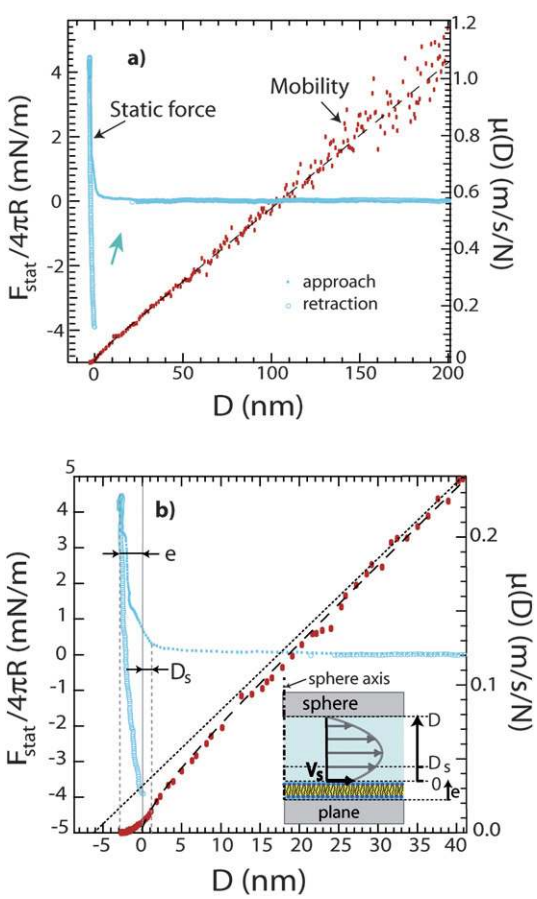

Fig. 5 (a) Static force and mobility measured as a function of the sphere-plane distance on a DOPC bilayer at the first approach. The dashed line is the best fit of $\mu(D)$ with a no-slip boundary condition on the sphere and a slip length $l_s = 6$ nm on the bilayer. (b) Zoom close to the contact on the first approach of the sphere. The dotted line is the linear extrapolation of the mobility measured at large distances. The inset represents schematically the flow of water on the DOPC bilayer.

As the mobility $\mu(D)$ does not vary as a straight line with D, the boundary velocity is no longer a zero velocity. We describe the mobility by assuming a sliding velocity V_s of the DOPC/water interface described by the Navier partial slip boundary condition $V_s = l_s \partial V(z)/\partial z$, where l_s is the Navier length and $b = \eta_w/l_s$ the associated fluid friction coefficient:

$$\mu(D) = \frac{D}{6\pi\eta_w R^2 f_a^*(D/l_s)}$$
$$f_a^*(x) = \frac{1}{4}\left(1 + \frac{6x}{4}[(1+4x)\ln(1+1/4x) - 1]\right) \quad (2)$$

f^*_a is the theoretical expression for an asymmetric system with a no-slip boundary condition on one side (the sphere) and a mobile boundary on the other.[23] The agreement is excellent (dashed line in Fig. 5b) and provides a slip length $l_s = 6 \pm 0.5$ nm. The slip length measured corresponds to an overall friction coefficient $b = 1.7 \pm 0.3\ 10^5$ Pa.s/m characterizing the sliding of the supported DOPC membrane.

IV. Discussion

This friction coefficient found on the DOPC bilayer is two to three orders of magnitude lower than the typical range of experimental values reported in the literature, obtained either through lipid diffusion or through dynamics of deformation of vesicles for the intermonolayer friction.[8,18,24–26] It is also one hundred times lower than the direct measurement performed by Jonsson *et al.* for egg-PC SLBs on glass. The systems are however different: egg-PC is a mixture of fluid-like and solid-like lipids of different heights, features which could increase the friction compared to a homogeneous fluid DOPC bilayer.

In contrast our result lies much closer to molecular dynamics simulations of sheared bilayers.[27] This raises the question of the actual origin of the friction measured in direct measurements. In lipid diffusion measurements, different friction mechanisms add up to lower the lipid mobility and the diffusion coefficient reflects the largest friction at play. In the direct measurements to the contrary, the overall tangential motion is the sum of all sliding motions, therefore the friction coefficient is dominated by the weakest coupling. There are in principle three sliding motions possible under a shear stress, associated with three friction coefficients: the inner monolayer on the Pyrex surface (b_{ms}), the monolayer/monolayer sliding (b_{mm}), and the water slippage onto the outer monolayer (b_{wm}). Among these potential sliding motions, we expect the slip of water on the outer monolayer to be negligible. First it is usually observed that water does not slip on hydrophilic surfaces.[28] Second the absence of slippage on hydrophilic surfaces is heavily supported by theoretical understanding of interfacial hydrodynamics.[29] Finally a no-slip condition is found on the DPPC bilayers, which have the same polar heads as DOPC.[21] Therefore the possible sliding mechanisms are the sliding of the bilayer on the Pyrex substrate, and the monolayer/monolayer sliding. The measured friction coefficient b is the harmonic average of the associated friction coefficients:

$$1/b = 1/b_{ms} + 1/b_{mm} \quad (3)$$

We have a further insight on the relative importance of these two mechanisms by analyzing the subsequent cycles of approach-retraction of the sphere onto the DOPC bilayer. In all the experiments we have performed, the first approach is singular and differs, as opposed to DPPC, from the subsequent cycles which are all reproducible. In all the subsequent cycles, we find that *any attempt* to fit the viscous damping with a no-slip boundary condition on the sphere fails utterly, even when the position of the hydrodynamic origin is adjusted as a free parameter (see Fig. 6). In order to account for the measured damping, we have to assume an *identical* boundary condition on the sphere and on the plane:

$$\mu(D) = \frac{D}{6\pi\eta_w R^2 f_s^*(D/l_s)}$$
$$f_s^*(x) = \frac{x}{3}\left[\left(1+\frac{x}{6}\right)\ln\left(1+\frac{6}{x}\right)-1\right] \quad (4)$$

with f^*_s the theoretical expression for a system with symmetric boundary conditions.[23] The agreement obtained is excellent, and corresponds to a slip length $l_s = 6$ nm equal to the one obtained on the first approach.

This behaviour suggests that a piece of bilayer has been ripped off the plane on the first approach and covers the sphere, whereas the defect left behind is healed quickly enough so that the bilayer is reconstituted at the next cycle (Fig. 7). Similar behaviour was obtained by Tiberg *et al.* in their AFM study of supporter DOPC bilayers.[19] This picture is also supported by the behaviour of the static force in the reproducible cycles: the steric repulsive force at the entrance into the contact reaches a maximum value followed by two successive jumps of the sphere toward the plane (see Fig. 6b) of cumulated size 6–7 nm, comparable to the thickness of two DOPC bilayers. Thus when the two SLBs enter into contact they are able to sustain only a weak maximum load of 11μN before the penetration of the sphere through the two bilayers. The latter occurs in two steps, each one corresponding to the expulsion of the equivalent of one bilayer out of the contact region, as seen by the two successive jumps of the static force. An upper boundary of the maximum normal pressure that the SLBs can stand without penetration is estimated from the force threshold (11μN) assuming a Hertz contact between the sphere and the plane (with the Young's modulus of silica $E = 60$ GPa). The value of this maximal normal pressure, of 4.5 MPa, underlines the fragility of the DOPC supported bilayer.

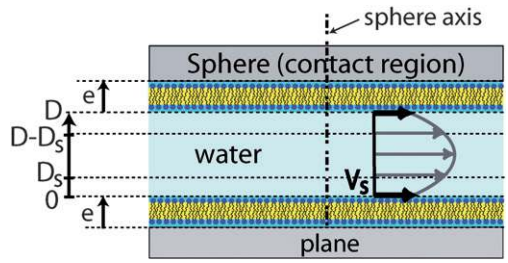

Fig. 7 Schematic representation of the flow of water on a DOPC bilayer and the associated distances in the symmetric case.

As already described by Israelachvili,[30] two different scenarios are conceivable for the penetration of the sphere into the two bilayers. In the first scenario (Fig. 8a), one membrane (probably the one on the sphere because of its probable lower density) "ruptures" and is expelled out of the contact. Then the second membrane behaves in the same way until the sphere enters into contact with the plane. This double rupture scenario does not require any monolayer/monolayer sliding and thus is expected if the friction coefficient b_{ms} of the inner monolayer onto the Pyrex surface is much lower than the coefficient b_{mm} for the monolayer/monolayer friction. In this case we would measure $b_{ms} \simeq b \simeq 2 \times 10^5$ Pa.s/m. As Israelachvili concludes, this scenario which involves similar steps should show a similar activation barrier or static force threshold for bilayer ejection, which is not the case in Fig. 6. Therefore it is likely that we do not have the double rupture scenario. However we cannot completely rule out this possibility since the two bilayers are not necessarily totally similar. The second scenario (Fig. 8b) involves the hemifusion of the two outer monolayers, which requires monolayer/monolayer sliding, then the rupture and expulsion of the new bilayer formed by the inner monolayers, which involves monolayer/Pyrex sliding. From the force thresholds on Fig. 6 the second step (rupture) appears easier than hemifusion (first step) from the point of view of resistance to normal stress, therefore the

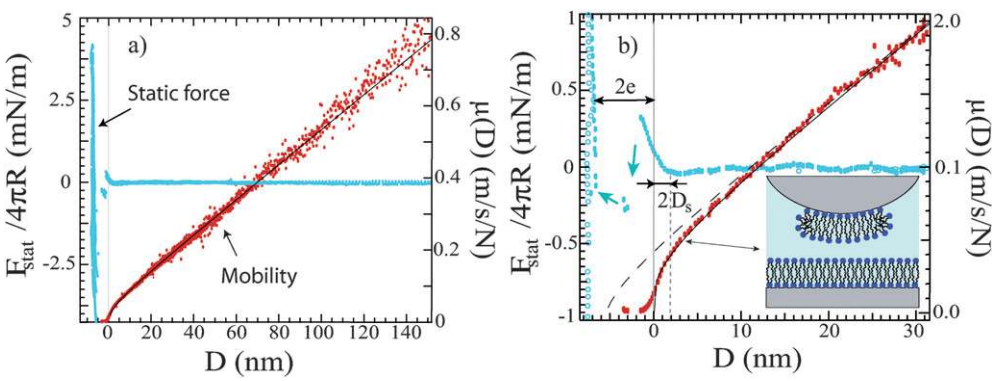

Fig. 6 (a) Static force and mobility measured as a function of the sphere-plane distance on a DOPC bilayer for the subsequent cycles (four cycles are superimposed) for a sphere of radius $R = 3$ mm. (b) Zoom on the first 30 nm of one cycle. The arrows on the static force symbolize the two jumps of the sphere toward the contact. The continuous black line is the best fit of the damping, obtained with *the same* slip boundary condition on the sphere and on the plane. The slip length is $l_s = 6$ nm. For comparison the dashed line is the best "non-symmetric" fit with a no-slip boundary condition on the sphere and a boundary slip on the plane. For this "non-symmetric" fit the hydrodynamic origin has to be shifted at $z_o = -5.5$ nm.

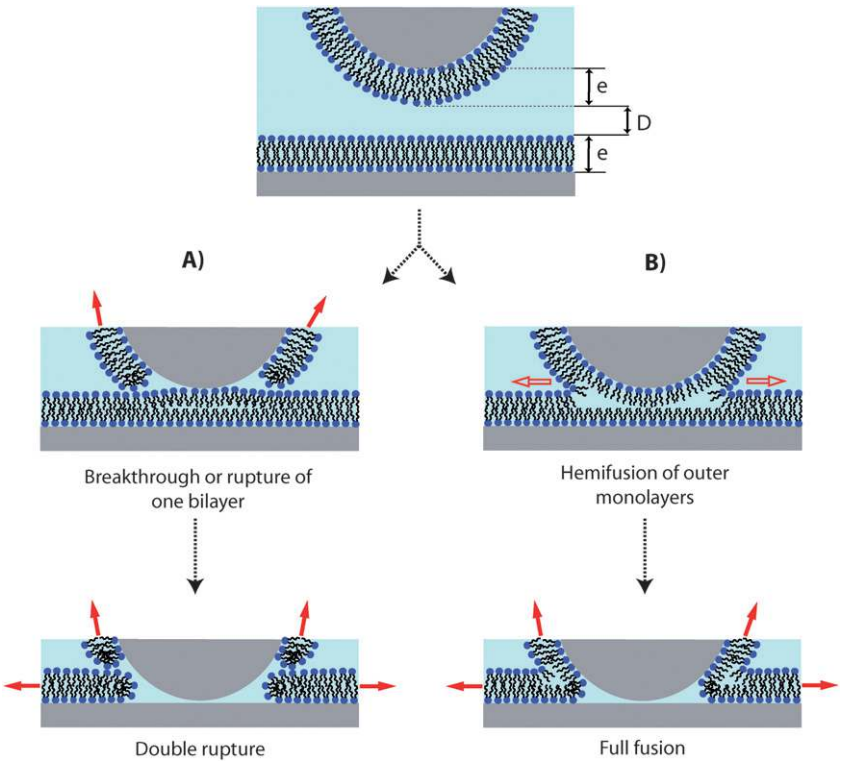

Fig. 8 Schematic representation of the two possible mechanisms for penetration of the sphere into the two DOPC bilayers. The (A) mechanism requires only the sliding of bilayers on Pyrex (solid arrows) and the (B) mechanism involves both a monolayer/monolayer sliding (open arrows) and a sliding of bilayers on Pyrex (solid arrows).

monolayer/Pyrex friction should not be much larger than the monolayer/monolayer friction. In the case of this second scenario, we can conclude that both friction mechanisms have a similar magnitude. More precisely, by estimating $b_{mm}/5 \leq b_{ms} \leq 5b_{mm}$ equation 3 provides bounds for the value of the DOPC monolayer/Pyrex friction coefficient. Thus, whatever the scenario, we can conclude that: 2×10^5 Pa.s/m $\leq b_{ms} \leq 10^6$ Pa.s/m

This magnitude is significantly low compared to typical values reported in the literature. However the available experimental determinations have been carried out on systems not exactly similar to ours. Indeed, the DOPC supported bilayers formed by the micelle method have been shown to be fragile and to present low resistance to AFM indentation.[16] Nevertheless, our result demonstrate the possibility of very low friction of lipid headgroups on a Pyrex surface. Super-lubricating effects have also been observed by Briscoe *et al.* on surfactant bilayers under water, and attributed to the hydration layers surrounding the headgroups.[31] We should mention that our results are not exactly comparable, as we evidence here a fluid friction behaviour under zero load, whereas Briscoe *et al.* probe solid friction under load. More work is needed for a better understanding of the relation between these two frictionnal properties.

V. Conclusion

In conclusion, the dynamic surface force apparatus used as a surface nanorheometer provides an original method to investigate the mechanical properties of supported lipid bilayers. Thanks to this nanorheology technique, we evidence the rigidity of DPPC bilayers both under tangential and normal stresses, in contrast to DOPC bilayers which exhibit a fluid response to a tangential stress and undergo a reversible rupture under normal stress. We also provide a direct mechanical measurement of the friction coefficient of a DOPC bilayer onto a glass supporting substrate. The latter is a fluid friction coefficient which has to be distinguished from solid friction between two rubbing surfaces. Compared to previous experimental estimations performed on related but not exactly similar systems, our results show a low friction coefficient of lipid headgroups onto Pyrex. This finding shows the same tendency as the super-lubricating effects reported by Briscoe *et al.* on surfactant bilayers under water.[31]

We expect that such a direct mechanical study of supported lipid bilayers should provide a significant contribution to the quantitative understanding of their bio-lubricating power and the solid friction properties of surfaces that they coat. Indeed the solid friction of surfaces coated by similar phospholipid layers to the ones studied in the present work have been investigated by Sfarghiu *et al.*[5,16] They found a much lower friction coefficient on DPPC bilayers than on DOPC ones, due to the fact that DOPC are more fragile and deteriorate under the sliding. This corroborates the work of Drummond *et al.* showing the increase of friction between surfactant bilayers undergoing hemifusion.[32] One could guess that a low fluid friction of the supported bilayer on its substrate should facilitate its tangential motion under normal load, thus lowering the pressure threshold for its rupture. Therefore we plan to study more comprehensively the relation between the tangential friction of supported bilayers on their substrate and their resistance to normal load, by investigating the

influence of physico-chemical parameters (such as the method of deposition, the lipid density, and the ion content of the solution) as well as the mechanical properties (curvature and rigidity) of the substrate. These results may participate in a better understanding of the very low fluid friction coefficients found in biolubrication phenomena, and have implications for future technological and biomedical applications.[6]

VI. Appendix—membrane deformation

The axisymmetric sliding of a DOPC membrane induces an oscillating deformation in the plane, proportional to the amplitude of the driving and associated with a spatial modulation of the lipid density which could induce non-linear effects. We estimate here the amplitude of the DOPC membrane deformation in the conditions of the experiment. The amplitude of the deformation $\varepsilon(r)$ at a distance r from the sphere-plane axis is related to the displacement $a_s(r)\cos\omega t$ of the membrane element by:

$$\varepsilon(r) = \frac{\mathrm{d}a_s(r)}{\mathrm{d}r} \quad a_s(r) = \frac{V_s(r)}{\omega} = \frac{\tilde{v}(r,0)}{\omega}$$

with $\tilde{v}(r,y)$ the amplitude of the oscillating flow velocity in the water film and (r, y) the cylindrical coordinates (see Fig. 1). The latter satisfy $0 \leq y \leq z = D + r^2/2R$ in the limit $D \ll R$. The flow profile is parabolic in y and obeys the mass conservation relation

$$\int_0^z \tilde{v}(r,y)dy = r\dot{D}/2 = rh_o\omega/2$$

For the sake of simplicity and because we can study more easily the linearity of the reproducible cycles, we assume here symmetric boundary conditions

$$\tilde{v}(r,0) = l_s\left(\frac{\partial\tilde{v}}{\partial y}\right)_{y=0} \quad \tilde{v}(r,z) = l_s\left(\frac{\partial\tilde{v}}{\partial y}\right)_{y=z}$$

The velocity profile is $\tilde{v} = (a_s\omega/zl_s)[z(y + l_s) - y^2]$ with

$$a_s = \frac{3rh_ol_s}{z(z+6l_s)}$$
$$\varepsilon(r) = \frac{3h_ol_s}{z(z+6l_s)}\left(1 - \frac{2r^2}{zR}\frac{z+3l_s}{z+6l_s}\right) \tag{5}$$

The deformation is plotted as a function of the radial distance r for various values of the sphere-plane distance in Fig. 9. It has a non-monotonic variation, and some parts of the membrane are compressed while other are extended. The maximum deformation, located on the sphere-plane axis, is:

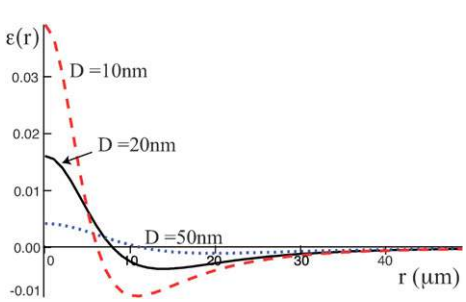

Fig. 9 Amplitude of the deformation of the DOPC bilayer as a function of the radial distance r, for various values of the sphere-plane distance.

$$\varepsilon_{max} = \frac{3l_sh_o}{D(D+6l_s)}$$

Thus large deformations are obtained only at small distances. However the ratio h_o/D of the driving amplitude to the sphere-plane distance has to be small in order to remain in the limit of linear response. In practice we limit the driving amplitude to $h_o/D \leq 0.1$. With this value the largest membrane deformation possible to probe is $\varepsilon_{max} \leq 5 \times 10^{-2}$. Within the limit $h_o/D \leq 0.1$ we have investigated the sphere mobility at various driving amplitude and have not found any non-linearity of the DOPC friction coefficient. We can also underline that the DPPC bilayer is too rigid to be deformed in this experiment by the axisymmetric solicitation.

Acknowledgements

We thank Jean-Paul Rieu and Magda Corneci for helpful discussions.

References

1 M. Tanaka and E. Sackmann, *Nature*, 2005, **437**, 656–663.
2 N. Malmstadt, M. A. Nash, R. Purnell and J. Schmidt, *Nano Lett.*, 2006, **6**, 1961–1965.
3 J. Taylor, K. Phillips and Q. Cheng, *Lab Chip*, 2007, **7**, 927–930.
4 B. A. Hills and B. D. Butler, *Ann. Biomed. Eng.*, 1985, **13**, 573.
5 A.-M. Trunfio-Sfarghiu, Y. Berthier, M.-H. Meurisse and J.-P. Rieu, *Tribol. Int.*, 2007, **40**, 1500–1515.
6 J. Klein, *Science*, 2009, **323**, 47–48.
7 L. Tamm and H. McConnell, *Biophys. J.*, 1985, **47**, 105–113.
8 R. Merkel, E. Sackmann and E. Evans, *J. Phys.*, 1989, **50**, 1535–1555.
9 T. Baumgart and A. Offenhausser, *Biophys. J.*, 2002, **83**, 1489–1500.
10 M. Hetzer, S. Heinz, S. Grage and T. M. Bayerl, *Langmuir*, 1998, **14**, 982–984.
11 E. Evans and E. Sackmann, *J. Fluid Mech.*, 1988, **194**, 553.
12 S. A. Shkulipa, W. K. den Otter and W. J. Briels, *Biophys. J.*, 2005, **89**, 823–829.
13 W. K. den Otter and S. A. Shkulipa, *Biophys. J.*, 2007, **93**, 423–433.
14 P. Jonsson, J. Beech, J. Tegenfeldt and F. Hook, *Langmuir*, 2009, **25**, 6279–6286.
15 C. Drummond, G. Marinov and P. Richetti, *Langmuir*, 2008, **24**, 1560–1565.
16 A.-M. Trunfio-Sfarghiu, Y. Berthier, M.-H. Meurisse and J.-P. Rieu, *Langmuir*, 2008, **24**, 8765–8771.
17 F. Restagno, J. Crassous, E. Charlaix, C. Cottin-Bizonne and M. Monchanin, *Rev. Sci. Instrum.*, 2002, **73**, 2292–2297.
18 K. Seu, A. Pandey, F. Haque, E. Proctor, A. Ribbe and J. Hovis, *Biophys. J.*, 2007, **92**, 2445–2450.
19 L. Grant and F. Tiberg, *Biophys. J.*, 2002, **82**, 1373–1385.
20 Y. Liu and J. Nagle, *Phys. Rev. E: Stat., Nonlinear, Soft Matter Phys.*, 2004, **69**, 040901.
21 B. Cross, A. Steinberger, C. Cottin-Bizonne, J. Rieu and E. Charlaix, *Europhys. Lett.*, 2006, **73**, 390–395.
22 F. Tiberg, I. Harwigsson and M. Malmsten, *Eur. Biophys. J.*, 2000, **29**, 196.
23 O. Vinogradova, *Langmuir*, 1995, **11**, 2213–2220.
24 E. Evans and A. Yeung, *Chem. Phys. Lipids*, 1994, **73**, 39–56.
25 R. Raphael and R. Waugh, *Biophys. J.*, 1996, **71**, 1374–1388.
26 J.-B. Fournier, N. Khalifat, N. Puff and M. Angelova, *Phys. Rev. Lett.*, 2009, **102**, 018102.
27 W. K. den Otter and S. A. Shkulipa, *Biophys. J.*, 2007, **93**, 423–433.
28 C. Cottin-Bizonne, A. Steinberger, B. Cross, O. Raccurt and E. Charlaix, *Langmuir*, 2008, **24**, 1165–1172.
29 L. Bocquet and J.-L. Barrat, *Soft Matter*, 2007, **3**, 685.
30 J. Wong, C. Park, M. Seitz and J. N. Israelachvili, *Biophys. J.*, 1999, **77**, 1458–1468.
31 W. Briscoe, S. Titmuss, F. Tiberg, R. Thomas, D. McGillivray and J. Klein, *Nature*, 2006, **444**, 191–193.
32 C. Drummond, G. Marinov and P. Richetti, *Langmuir*, 2008, **24**, 1560–1565.